Inorganic Chemistry

pubs.acs.org/IC

Forum Article

Role of the Precursor Composition in the Synthesis of Metal Ferrite Nanoparticles

Hogeun Chang,[†] Byung Hyo Kim,[†] Suk Gyu Lim, Hayeon Baek, Jungwon Park,* and Taeghwan Hyeon*

Cite This: https://dx.doi.org/10.1021/acs.inorgchem.0c03567

Read Online

ACCESS | Metrics & More | Article Recommendations | Supporting Information

ABSTRACT: Ternary oxide nanoparticles have attracted much interest because of their intriguing properties, which are not exhibited by binary oxide nanoparticles. However, the synthesis of ternary oxide nanoparticles is not trivial and requires a fundamental understanding of the complicated precursor chemistry that governs the formation mechanism. Herein, we investigate the role of the chemical composition of precursors in the formation of ternary oxide nanoparticles via a combination of mass spectrometry, electron microscopy with elemental mapping, and thermogravimetric analysis. Mn^{2+}, Co^{2+}, and Ni^{2+} ions easily form bimetallic-oxo clusters with Fe^{3+} ions with a composition of $MFe_2O(oleate)_6$ (M = Mn, Co, Ni). The use of clusters as precursors leads to the successful synthesis of monodisperse metal ferrite nanoparticles (MFe_2O_4). On the contrary, zinc- or copper-containing complexes are formed independently from iron-oxo clusters in the precursor synthesis. The mixture of complexes without a bimetallic-oxo core yields a mixture of two different nanoparticles. This study reveals the importance of the precursor composition in the synthesis of ternary oxide nanoparticles.

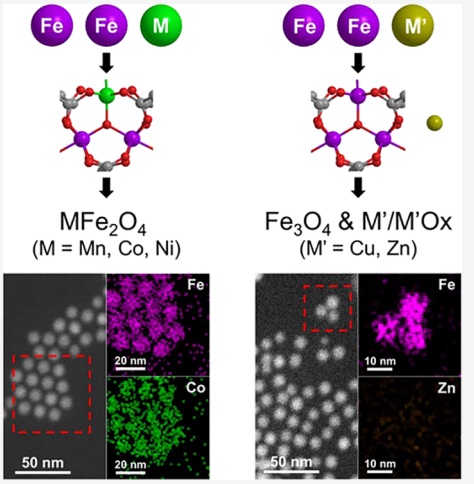

INTRODUCTION

Thermal decomposition of precursors in the presence of surfactants, a process referred to as colloidal synthesis, is an efficient method for synthesizing high-quality nanoparticles.[1,2] The formation of nanoparticles via colloidal synthesis is governed by the reaction chemistry of precursors at the early stage and interactions between the growing nanoparticles and surfactant molecules in the following stage.[3,4] Depending on the structures of the precursor molecules and the kinetics of their decomposition to generate monomers, nanoparticle growth can follow different formation mechanisms.[5−13] For example, the use of reactive organometallic compounds or metal carboxylate/amine complexes as precursors results in specific growth kinetics,[9,14] structures,[7,10,15] and compositions[12] of the synthesized nanoparticles. NMR, ultraviolet−visible (UV−vis) absorption, and matrix-assisted laser desorption/ionization time-of-flight mass spectrometry (MALDI-TOF MS) have been used to characterize the species identified during the early stage of the nanoparticle formation.[14,16−20]

Ternary oxide nanoparticles, which have gained significant interest because of their unique properties not present in binary nanoparticles,[21−23] are also synthesized via colloidal synthesis. Indium−tin oxide nanoparticles display localized surface plasmon resonance absorption that can be regulated by an external electric bias, allowing their use in electrochromic devices.[24,25] The magnetic moments of spinel ferrite (MFe_2O_4) nanoparticle can be enhanced by introducing extra constituent metals other than Fe.[26−29] However, the colloidal synthesis of monodisperse ternary oxide nanoparticles was not always successfully synthesized by the simple mixing of two different metal precursors before the report of the synthesis of a uniform composition nanocrystal based on thermolysis by the Gupta group.[30−34] This is because the synthesis requires complicated precursor molecules including two metal constituents or multiple precursors with similar decomposition kinetics. Indeed, reaction products from two metal precursors (M and M′) usually yield a mixture of two metal oxide nanoparticles (MO_x and $M'O_y$) instead of forming ternary oxide nanoparticles (MM'_xO_y).[35−37] These challenges in the synthesis of ternary oxide nanoparticles can be overcome by a fundamental understanding of the reaction chemistry of precursors and their influence on the composition of the final nanoparticles. Inspired by the previous studies that elucidated the role of iron oleate precursors in the synthesis of binary iron oxide nanoparticles, we correlated the chemical formula of the

Special Issue: Inorganic Chemistry of Nanoparticles

Received: December 6, 2020

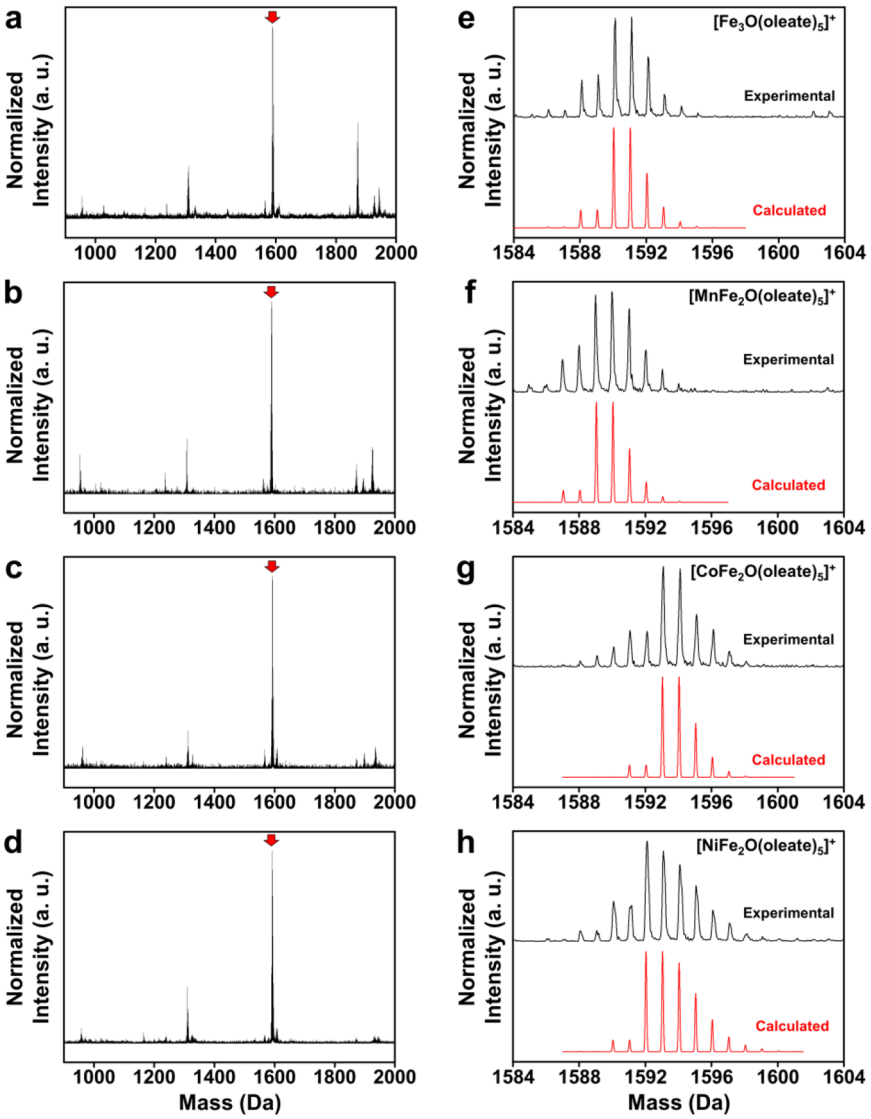

Figure 1. Mass characterization of bimetallic-oxo oleate precursor. (a–d) MALDI-TOF MS spectra. (e–h) Isotope calculation of the main peak. The experimental (black) and calculated (red) peaks show clear correspondence. (a and e) Fe^{3+}-oleate showing $[Fe_3O(oleate)_5]^+$, (b and f) Mn^{2+}-Fe^{3+}-oleate showing $[MnFe_2O(oleate)_5]^+$, (c and g) Co^{2+}-Fe^{3+}-oleate showing $[CoFe_2O(oleate)_5]^+$, and (d and h) Ni^{2+}-Fe^{3+}-oleate showing $[NiFe_2O(oleate)_5]^+$.

precursors and the compositions of synthesized nanoparticles with each other in the synthesis of ternary nanoparticles.[38]

Herein, we analyze the compositions of the precursors in the formation of diverse ternary oxide nanoparticles and find that the precursor composition is a critical factor in the successful incorporation of two constituent metals in the synthesized ternary oxide nanoparticles. Spinel ferrite, one of the most representative ternary oxide materials, is chosen as a model system. The precursors for $MnFe_2O_4$, $CoFe_2O_4$, and $NiFe_2O_4$ have compositions of $MFe_2O(oleate)_6$ (M = Mn, Co, Ni), and metal ferrite nanoparticles are successfully synthesized from the bimetallic-oxo clusters (type I). On the contrary, the precursors for $ZnFe_2O_4$ and $CuFe_2O_4$ cannot be synthesized as bimetallic-oxo clusters but as a mixture of metal oleate complexes, which yields a mixture of two different nanoparticles (type II).

MATERIALS AND METHODS

Materials. Iron(III) chloride hexahydrate (98%), magnesium(II) chloride hexahydrate (99%), cobalt(II) chloride hexahydrate (98%), nickel(II) chloride hexahydrate (98%), copper(II) chloride dehydrate (99%), zinc(II) chloride (98%), oleic acid, 1-octadecene (1-OD), and 9-nitroanthracene (9-NA) were purchased from Sigma-Aldrich. Sodium oleate (95%) was purchased from Tokyo Chemical Industry (TCI). Ethanol, chloroform, and *n*-hexane were purchased from Samchun Chemicals.

Synthesis of Metal Oleate Complexes. The synthesis of metal oleate complexes proceeded based on the previous reports.[32,39,40] To synthesize Fe^{3+}-oleate complexes, iron(III) chloride hexahydrate (20 mmol) and sodium oleate (60 mmol) were added to a mixture of 70 mL of hexane, 40 mL of ethanol, and 30 mL of deionized water and stirred for 4 h at 55 °C. Similarly, to synthesize M^{2+}-oleate complexes, metal(II) chloride hexahydrate (20 mmol) and sodium oleate (40 mmol) were mixed in the same solvent and at the same temperature conditions. After the reaction, the hexane phase was separated using a separation funnel and washed three times with deionized water. Finally, hexane was evaporated overnight in a vacuum.

https://dx.doi.org/10.1021/acs.inorgchem.0c03567
Inorg. Chem. XXXX, XXX, XXX−XXX

Synthesis of Mixed-Metal Oleate Complexes. Mixed-metal oleate complexes were synthesized based on the previously reported method with a slight modification.[33] The stoichiometry of the reactants was considered for charge balance of the final product. To synthesize M^{2+}−Fe^{3+}-oleate complexes, 6.67 mmol of metal(II) chloride, 13.33 mmol of iron(III) chloride hexahydrate, and 53.33 mmol of sodium oleate were dissolved in the same solvent mixture. (i.e., M^{2+}:Fe^{3+}:oleate$^-$ = 1:2:8). The same process steps were followed for separation and evaporation.

Synthesis of Metal Ferrite Nanoparticles. Metal ferrite nanoparticles were synthesized via a well-known heating process.[3,4,33,39] A total of 1.9 g of metal oleate or mixed-metal oleate complexes, 0.285 g of oleic acid, and 10.0 g of 1-OD were mixed and degassed at 70 °C for 1 h. The mixture was heated to 320 °C at a heating rate of 3.3 °C/min and subsequently held at that temperature for 30 min in an inert atmosphere. After the reaction, the solution was rapidly cooled and centrifuged with ethanol to remove unreacted reactants and byproducts. The final product was dispersed in a nonpolar solvent such as hexane or chloroform.

Mass Characterization. MALDI-TOF MS data were obtained using a Voyager-DE STR Biospectrometry Workstation manufactured by Applied Biosystems Inc. at the National Center for Inter-University Research Facilities (NCIRF) at Seoul National University. Angiotensin I [M_{mi} (mass of maximum intensity) = 1296.6853 Da], adrenocorticotropic hormone (ACTH) 1−17 corticotropin-like intermediate peptide (CLIP; M_{mi} = 2093.0867 Da), ACTH 18−39 CLIP (M_{mi} = 2465.1989 Da), ACTH 7−38 CLIP (M_{mi} = 3657.9294 Da), and insulin (M_{mi} = 5730.6087 Da) were used as calibrants. Concentrated 9-NA in chloroform was used as a matrix. A pulsed-nitrogen laser (337 nm, 3 ns pulses) at a power setting of 60−70% induced desorption and ionization of metal oleate complexes. A 20 kV potential was applied, which accelerated the positive ions after desorption and ionization. The reflector mode was used for detailed MS.

Transmission Electron Microscopy (TEM), Scanning Transmission Electron Microscopy (STEM), and Energy-Dispersive X-ray Spectroscopy (EDS). TEM and STEM were performed using a JEOL JEM 2100F/HR instrument operated at 200 kV. EDS spectra and elemental mapping were acquired using an Oxford EDS system with an 80 mm^2 detector (Oxford Instruments Analytical Ltd., U.K.). Samples were prepared by placing a drop of diluted solution on the TEM grid (copper or gold) and drying it overnight prior to observation.

Optical Characterization. Fourier transform infrared (FT-IR) and optical absorption spectra of the metal oleate complexes were acquired using a Bruker VERTEX 70 V spectrometer and a CARY 5000E UV−vis−near-IR (NIR) spectrophotometer.

Thermogravimetric Analysis (TGA). TGA of the metal oleate complexes was performed in an air atmosphere at a 10 °C/min rate up to 600 °C using an SDT Q600 instrument.

RESULTS AND DISCUSSION

Characterization of Precursors: Bimetallic-Oxo Complexes (Type I). The precursors of the bimetallic ferrite nanoparticles were prepared by reacting metal(II) chloride, iron(III) chloride, and sodium oleate in the ratio 1:2:8. Late-transition-metal ions in the fourth row of the Periodic Table with oxidation states of 2+, including Mn^{2+}, Co^{2+}, Ni^{2+}, Cu^{2+}, and Zn^{2+}, were used to investigate the role of precursors in the synthesis of metal ferrite nanocrystals. The bimetallic precursors were characterized by MALDI-TOF MS, which provided the precise molecular weight of inorganic complexes or clusters with minimal fragmentation. The MALDI-TOF MS spectra of the Fe^{3+}-oleate complexes show main peaks with a mass-to-charge ratio (m/z) of 1590 Da (Figure 1a). The Mn^{2+}−Fe^{3+}-oleate complexes (Figure 1b) and Co^{2+}−Fe^{3+}-oleate complexes (Figure 1c) have MS spectra with main peak positions of 1589 and 1593 Da, respectively. Because the atomic weights of manganese and cobalt are 55 and 59 Da, respectively, their atomic weight differences of −1 and +3 Da relative to iron (56 Da) indicate that each complex contains one divalent metal ion. Identification of the Ni^{2+}−Fe^{3+}-oleate complexes by the peak positions in MALDI-TOF MS spectra is intricate because of the number of nickel isotopes; thus, isotope calculations are required (Figure 1d). Isotope calculations of the main peaks at 1590 Da of Fe^{3+}-oleate complexes confirm that the chemical structure of the complexes is $[Fe_3O(oleate)_5]^+$, where oleate is a long-chain carboxylate ion with a chemical formula of $C_{18}H_{33}O_2^-$ (Figure 1e). In the same way, the main peaks of Mn^{2+}−Fe^{3+}-oleate, Co^{2+}−Fe^{3+}-oleate, and Ni^{2+}−Fe^{3+}-oleate complexes are consistent with the calculated isotope peaks of $[MnFe_2O(oleate)_5]^+$, $[CoFe_2O(oleate)_5]^+$, and $[NiFe_2O(oleate)_5]^+$, respectively (Figure 1f−h). Other major peaks can also be assigned as $[MFe_2O(oleate)_n]^+$ (n = 4 or 6) with the mass difference corresponding to one oleate ion from the main peak (Figure S1).

The trinuclear-oxo carboxylate complex $MFe_2O(carboxylate)_6$ is known as a stable triangular structure.[41−47] $[MFe_2O(oleate)_5]^+$ can be assigned as the ionized product of the $MFe_2O(oleate)_6$ complexes through the detachment of one oleate ligand during laser desorption. In the $MFe_2O(oleate)_6$ structure, two trivalent iron ions and one divalent transition-metal ion are bonded to the centered μ_3-oxygen, while six oleate ($C_{18}H_{33}O_2^-$) ligands are bridging two of the metal ions. In the case of the $[Fe_3O(oleate)_6]^+$ complex, the charges of the iron atoms are delocalized at room temperature;[43,47] thus, each iron atom of the complexes can be regarded as identical. Therefore, the $[Fe_3O(oleate)_6]^+$ complex can be categorized as a D_{3h} point group, while the other trinuclear-oxo oleate complexes are categorized as C_{2v} point groups.

Characterization of Precursors: Mixture of Complexes (Type II). Unlike the $MnFe_2O(oleate)_6$, $CoFe_2O(oleate)_6$, and $NiFe_2O(oleate)_6$, the major product of the reaction between zinc(II) chloride, iron(III) chloride, and sodium oleate is not $ZnFe_2O(oleate)_6$. The peak distribution of the main MALDI-TOF MS peaks of the products does not match the isotope distribution of $[ZnFe_2O(oleate)_5]^+$ but matches the isotope peaks of $[Fe_3O(oleate)_5]^+$ (red lines in Figure 2). This result implies that the Zn^{2+} ions do not readily form bimetallic-oxo complexes, $MFe_2O(oleate)_6$. Instead, they form triiron-oxo oleate clusters and zinc-containing complexes, separately (Figure S2). A similar phenomenon is observed in the MALDI-TOF MS spectra of Cu^{2+}−Fe^{3+}-oleate complexes, which correspond to $[Fe_3O(oleate)_5]^+$ rather than $[CuFe_2O(oleate)_5]^+$ (blue lines in Figure 2). Compared to the $CuFe_2O$ or $ZnFe_2O$ clusters synthesized with short ligands (C_2), formation of the $CuFe_2O$ and $ZnFe_2O$ core structures with long ligands (C_{18}) is unfavorable.[48]

The structural difference between the type I mixed-metal oleate and type II complexes is supported by the optical characterization data (Figure 3). IR absorption at a wavenumber of 600 cm^{-1} corresponds to the characteristic asymmetric stretching of the triangular Fe_3O core, which has three trivalent iron atoms (black line in Figure 3b).[49] When one of the iron atoms in the Fe_3O core is substituted by divalent atoms, the triangular C_3 symmetry is broken and the point group is changed from D_{3h} to C_{2v}. The symmetry breakage results in a peak splitting of the asymmetric vibration IR peak (~600 cm^{-1} for the D_{3h} point group) to ~550 and ~720 cm^{-1}.[50] The IR spectra of the Mn^{2+}−Fe^{3+}-oleate, Co^{2+}−

https://dx.doi.org/10.1021/acs.inorgchem.0c03567
Inorg. Chem. XXXX, XXX, XXX−XXX

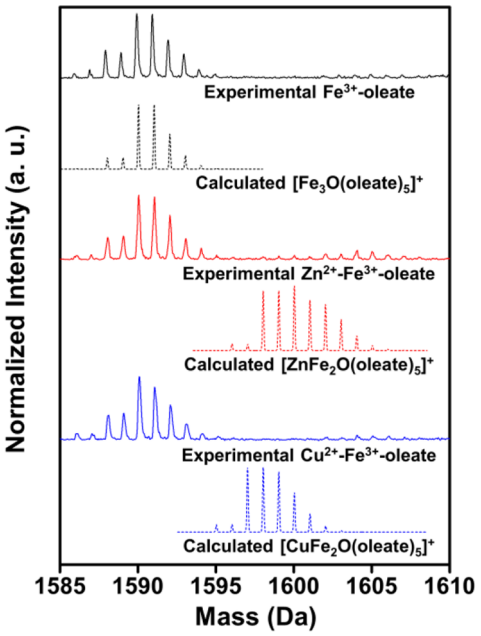

Figure 2. Mass characterization of mixed-metal oleate precursors. The experimental (solid line) and calculated (dotted line) peaks showing zinc and copper cannot be synthesized into the MFe_2O (M = Zn, Cu) cluster structure but show formation of the $[Fe_3O(oleate)_5]^+$ structure.

Fe^{3+}-oleate, and Ni^{2+}−Fe^{3+}-oleate complexes have absorption peaks at ∼530 cm^{-1}, indicating the successful formation of mixed metallic MFe_2O cores. The 720 cm^{-1} peaks are usually not distinctive because the peak is overlapped with strong C−H bending. On the contrary, the Zn^{2+}−Fe^{3+}-oleate and Cu^{2+}−Fe^{3+}-oleate complexes do not have strong absorption at ∼550 cm^{-1}, representing the absence of the mixed metallic MFe_2O cores with a C_{2v} point group. Rather, they show small peaks at ∼600 cm^{-1}, which may be attributed to Fe_3O with a D_{3h} point group. Strong absorption at 950 nm of the Mn^{2+}−Fe^{3+}-oleate, Co^{2+}−Fe^{3+}-oleate, and Ni^{2+}−Fe^{3+}-oleate complexes also represents the formation of MFe_2O cores (Figure 3c).[38,46]

The thermodynamic properties of the M^{2+}−Fe^{3+}-oleate complexes are further characterized by TGA. It has been reported that the divalent metal carboxylate complexes show higher decomposition temperature (∼490 °C) than the trivalent metal carboxylate complexes with triangular M_3O cores (∼370 °C; Figure S3).[51,52] The TGA curves of the Mn^{2+}−Fe^{3+}-oleate, Co^{2+}−Fe^{3+}-oleate, and Ni^{2+}−Fe^{3+}-oleate complexes display trends similar to those of the TGA curves of the iron oleate complexes (Figure S3a). The marginal difference in the decomposition temperature (∼10 °C) is presumably due to the different strengths of the metal−ligand bonds. In contrast, the TGA curves of the Zn^{2+}−Fe^{3+}-oleate complexes and Cu^{2+}−Fe^{3+}-oleate lie between the Fe^{3+}-oleate and divalent metal oleate complexes (Figure S3b), implying mixing of the trivalent oleate complexes and divalent metal oleate complexes. The combinatory measurements by MALDI-TOF MS, FT-IR, UV−vis−NIR, and TGA confirm that the manganese, cobalt, and nickel atoms reacted with iron atoms to form bimetallic $MFe_2O(oleate)_6$ complexes, while zinc and copper form a mixture of metal oleate and $Fe_3O(oleate)_6$ from the synthesis of the precursors for the metal ferrite nanoparticles.

Synthesis of Metal Ferrite Nanoparticles. Highly monodisperse iron oxide nanoparticles with sizes of 12 nm can be synthesized from thermal decomposition of the iron oleate precursors at 320 °C in an inert atmosphere (Figures 4a and S4a). Monodisperse manganese ferrite nanoparticles (Figures 4b and S4b), cobalt ferrite nanoparticles (Figures 4c and S4c), and nickel ferrite nanoparticles (Figures 4d and S4d) are also synthesized via the same synthetic protocol starting from $MnFe_2O(oleate)_6$, $CoFe_2O(oleate)_6$, and $NiFe_2O(oleate)_6$ precursors, respectively. The nanoparticle synthesis is reproducible, as confirmed by the TEM images from different batches (Figure S5). The successful formation of the ternary oxide is confirmed by elemental mapping with EDS (Figure 4e−h). The positions of the iron and manganese atoms of the nanoparticles synthesized from the $MnFe_2O$-

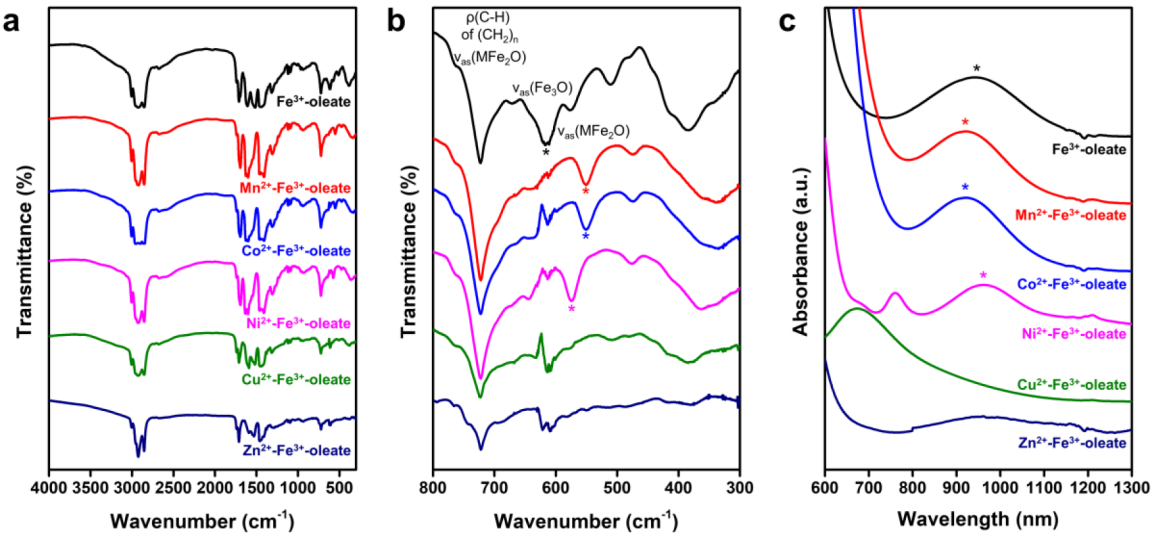

Figure 3. Optical characterization of the M^{2+}−Fe^{3+}-oleate complexes and the $Fe_3O(oleate)_6$ complex as a reference: (a and b) FT-IR and (c) UV−vis−NIR spectra. The spectra of Fe^{3+}-, Mn^{2+}−Fe^{3+}-, Co^{2+}−Fe^{3+}-, and Ni^{2+}−Fe^{3+}-oleates show characteristic peaks of the MFe_2O core, but the spectra of Cu^{2+}−Fe^{3+}- and Zn^{2+}−Fe^{3+}-oleates do not show the MFe_2O peaks.

https://dx.doi.org/10.1021/acs.inorgchem.0c03567
Inorg. Chem. XXXX, XXX, XXX−XXX

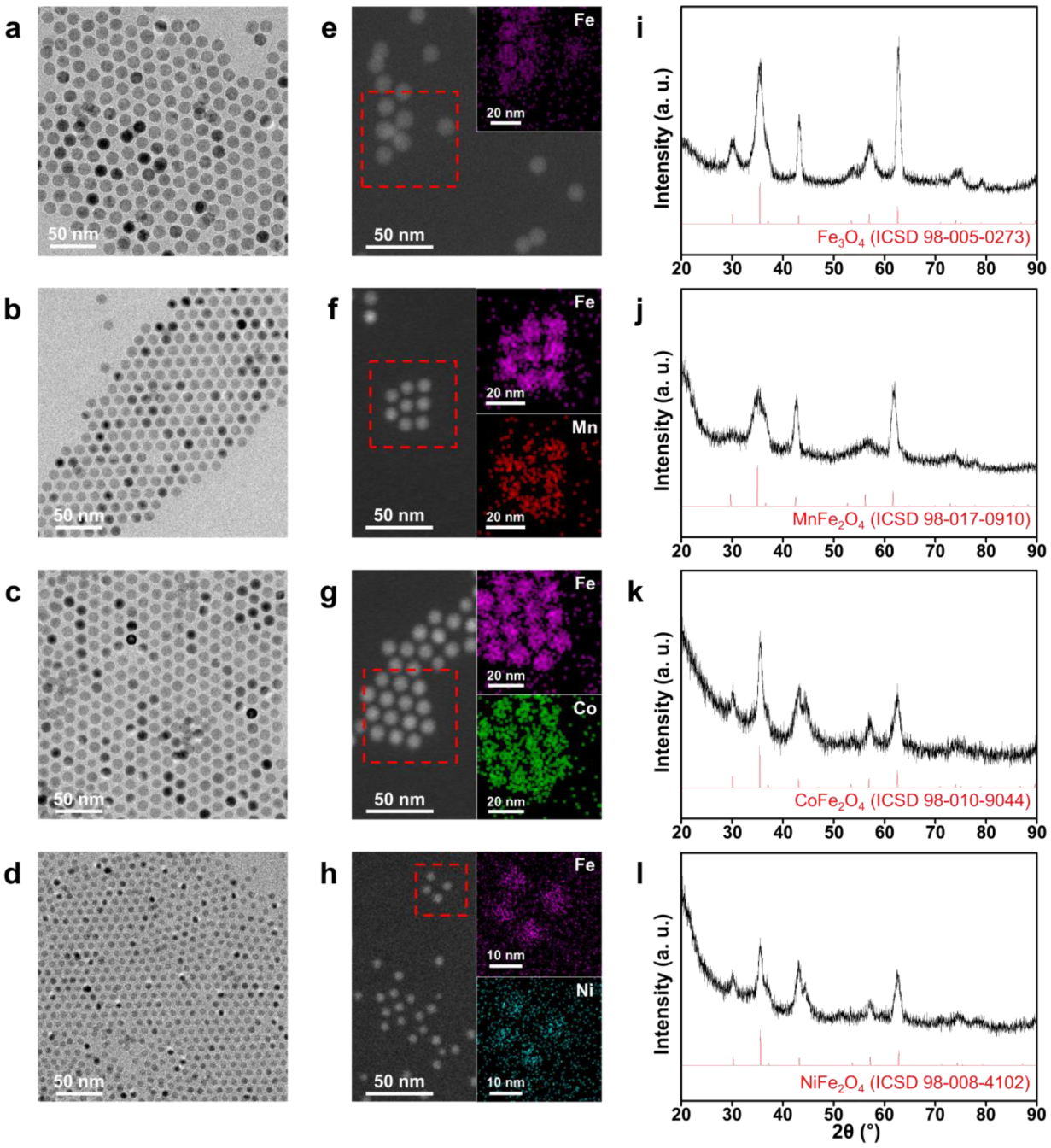

Figure 4. (a–d) TEM and (e–h) EDS images and (i–l) XRD patterns of nanoparticles synthesized from MFe_2O (M = Fe, Mn, Co, Ni) clusters as precursors. (a, e, and i) Fe_3O_4, (b, f, and j) $MnFe_2O_4$, (c, g, and k) $CoFe_2O_4$, and (d, h, and l) $NiFe_2O_4$ are synthesized from MFe_2O clusters.

$(oleate)_6$ complexes are overlapped with the positions of the nanoparticles, indicating that the nanoparticles contain both iron and manganese atoms (Figure 4f). In the same way, the elemental maps of nanoparticles synthesized from the $CoFe_2O(oleate)_6$ and $NiFe_2O(oleate)_6$ precursors confirm the successful formation of the ternary oxide nanoparticles (Figure 4g,h). X-ray diffraction (XRD) shows that the crystal structures of the ternary oxide nanoparticles are spinel ferrite structures (Figure 4i–l). Considering the overlap of divalent metals and iron in the EDS elemental mapping (Figures S6–S9), the crystal structures of the nanoparticles can be assigned as $MnFe_2O_4$ (Figure 4j), $CoFe_2O_4$ (Figure 4k), and $NiFe_2O_4$ (Figure 4l). The EDS data show 1:2 molar ratios between M (M = Mn, Co, Ni) and iron, supporting the formation of stoichiometric ternary metal ferrite structures.

In contrast, thermal decomposition of mixtures of metal oleate complexes does not form ternary oxide nanoparticles. EDS mapping of the nanoparticles synthesized from a mixture of zinc-containing and $Fe_3O(oleate)_6$ complexes reveals that the nanoparticles contain only iron atoms with a small portion of zinc atoms (Figures 5a,b and S10). The separation of iron- and zinc-containing nanoparticles is confirmed by XRD measurement. The XRD patterns indicate that the sample is a mixture of spinel ferrite (Fe_3O_4) and ZnO (Figures 5c and S11 and Table S1). EDS mapping of nanoparticles synthesized from the mixture of Cu-containing precursors and Fe_3O-

https://dx.doi.org/10.1021/acs.inorgchem.0c03567
Inorg. Chem. XXXX, XXX, XXX–XXX

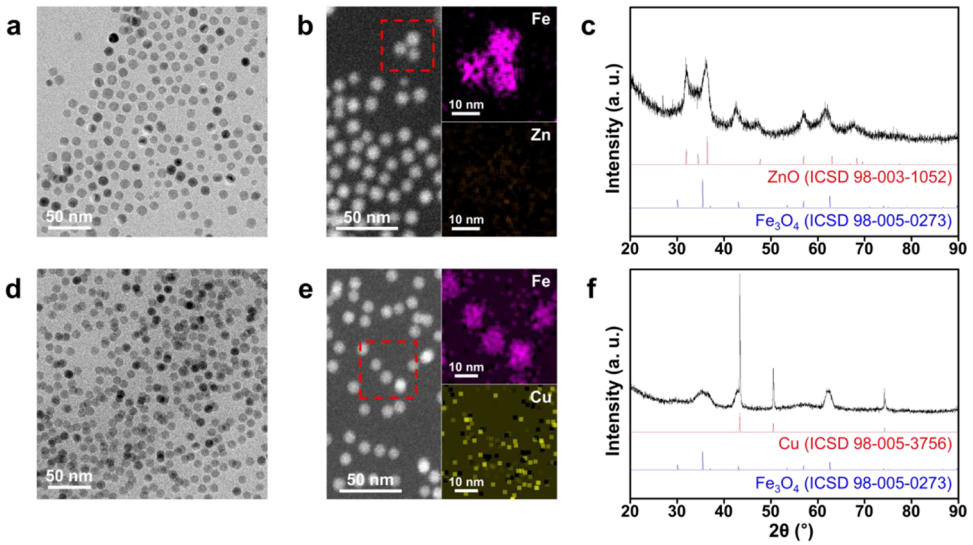

Figure 5. TEM and EDS images and XRD patterns of nanoparticles synthesized from (a–c) Zn^{2+}–Fe^{3+}-oleate and (d–f) Cu^{2+}–Fe^{3+}-oleate complexes.

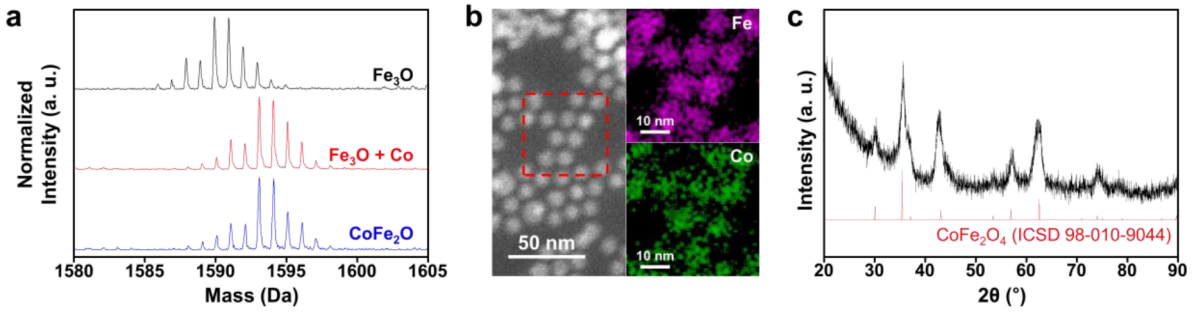

Figure 6. (a) Rearrangement of metal ions in the metal-oxo clusters. When Fe_3O clusters are reacted with Co^{2+}-oleate complexes, they clearly transform into $CoFe_2O$ clusters. (b) EDS and (c) XRD of the nanoparticles from a mixture of Fe^{3+}-oleate and Co^{2+}-oleate complexes.

$(oleate)_6$ complexes also verifies the marginal portion of copper atoms in the nanoparticles that contain iron (Figures 5d,e and S12). Actually, the reaction from a mixture of Cu-containing precursors and $Fe_3O(oleate)_6$ complexes yields a mixture of copper metal and spinel iron oxide (Fe_3O_4), as revealed by the XRD pattern (Figure 5f). The Cu^{2+} ions are reduced to zerovalent copper metal by CO or H_2 generated during thermal decomposition of the iron oleate complex.[3] Because the reduction potential of Cu^{2+} (0.34 V) is much higher than that of Zn^{2+} (−0.76 V), the Cu^{2+} precursor is readily reduced to copper metal, while the Zn^{2+} precursor is transformed to ZnO nanoparticles.[53]

The EDS mapping images and XRD patterns clearly reveal the relationship between the composition of the precursors and the resulting nanoparticles in the synthesis of ternary oxide nanoparticles. The use of bimetallic complexes as precursors, including $MnFe_2O(oleate)_6$, $CoFe_2O(oleate)_6$, and $NiFe_2O(oleate)_6$, results in metal ferrite nanoparticles. The metal–oxygen–iron (M–O–Fe) bonds remaining after the thermal decomposition process may guide the successful formation of metal ferrite nanocrystals. In contrast, when the metal and iron do not form a single cluster with a bimetallic-oxo core structure, this mixture of metal precursors cannot readily yield ternary oxide nanoparticles. Instead, the resulting nanoparticles are a mixture of two types of nanoparticles.

Rearrangement of the Metal Oleate Complexes. Ternary oxide nanoparticles have been synthesized not only from single bimetallic precursors but also from a mixture of two types of monometal precursors. Gupta et al. reported that the $CoFe_2O_4$ nanoparticles can be synthesized from a mixture of Fe^{3+}-oleate and Co^{2+}-oleate complexes.[32] The ternary oxide nanoparticles synthesized from the precursor mixture can also be explained by the formation of bimetallic precursors. We prepare the Fe^{3+}-oleate and Co^{2+}-oleate complexes separately, and then mix them in a 2:1 molar ratio. After mixing for 1 h at 70 °C, the Fe^{3+}-oleate and Co^{2+}-oleate mixture successfully rearranges to $CoFe_2O(oleate)_6$ complexes (Figure 6a). The resulting $CoFe_2O(oleate)_6$ complexes from the two metal oleate complexes can also be used as precursors for $CoFe_2O_4$ nanoparticles (Figures 6b,c and S13). The flexibility for rearrangement highlights the importance of the trinuclear-oxo core structure in the synthesis of ternary oxide nanoparticles.[38]

CONCLUSIONS

In this study, we investigate the correlation between the composition of precursors and final products in the synthesis of metal ferrite nanoparticles. When the precursors or early stage species form trinuclear-oxo clusters that contain both metal ions, ternary oxide nanoparticles are successfully synthesized. We believe that our study provides insight into the synthesis of monodisperse nanoparticles with complicated compositions.

https://dx.doi.org/10.1021/acs.inorgchem.0c03567
Inorg. Chem. XXXX, XXX, XXX–XXX

■ ASSOCIATED CONTENT

Supporting Information

The Supporting Information is available free of charge at https://pubs.acs.org/doi/10.1021/acs.inorgchem.0c03567.

Detailed MS spectra and TGA of metal oleate complexes, size distribution diagrams, supporting TEM images, EDS spectra of nanoparticles, XRD data, and d spacings of iron oxide nanoparticles (PDF)

■ AUTHOR INFORMATION

Corresponding Authors

Jungwon Park − *Center for Nanoparticle Research, Institute for Basic Science (IBS), Seoul 08826, Republic of Korea; School of Chemical and Biological Engineering and Institute of Chemical Process, Seoul National University, Seoul 08826, Republic of Korea;* orcid.org/0000-0003-2927-4331; Email: jungwonpark@snu.ac.kr

Taeghwan Hyeon − *Center for Nanoparticle Research, Institute for Basic Science (IBS), Seoul 08826, Republic of Korea; School of Chemical and Biological Engineering and Institute of Chemical Process, Seoul National University, Seoul 08826, Republic of Korea;* orcid.org/0000-0001-5959-6257; Email: thyeon@snu.ac.kr

Authors

Hogeun Chang − *Center for Nanoparticle Research, Institute for Basic Science (IBS), Seoul 08826, Republic of Korea; School of Chemical and Biological Engineering and Institute of Chemical Process, Seoul National University, Seoul 08826, Republic of Korea;* orcid.org/0000-0002-3322-898X

Byung Hyo Kim − *Department of Organic Materials and Fiber Engineering, Soongsil University, Seoul 06978, Republic of Korea*

Suk Gyu Lim − *School of Chemical and Biological Engineering and Institute of Chemical Process, Seoul National University, Seoul 08826, Republic of Korea*

Hayeon Baek − *Center for Nanoparticle Research, Institute for Basic Science (IBS), Seoul 08826, Republic of Korea; School of Chemical and Biological Engineering and Institute of Chemical Process, Seoul National University, Seoul 08826, Republic of Korea*

Complete contact information is available at: https://pubs.acs.org/10.1021/acs.inorgchem.0c03567

Author Contributions

†H.C. and B.H.K. contributed equally to this work. The manuscript was written through contributions of all authors. All authors have given approval to the final version of the manuscript.

Notes

The authors declare no competing financial interest.

■ ACKNOWLEDGMENTS

This work was supported by the Research Center Program of the IBS, Korea (Grant IBS-R006-D1). We especially thank Kyung Hee Lim of the NCIRF for assistance with MALDI-TOF MS measurements.

■ REFERENCES

(1) Park, J.; Joo, J.; Kwon, S. G.; Jang, Y.; Hyeon, T. Synthesis of monodisperse spherical nanocrystals. *Angew. Chem., Int. Ed.* **2007**, *46*, 4630−4660.

(2) Kwon, H. J.; Shin, K.; Soh, M.; Chang, H.; Kim, J.; Lee, J.; Ko, G.; Kim, B. H.; Kim, D.; Hyeon, T. Large-Scale Synthesis and Medical Applications of Uniform-Sized Metal Oxide Nanoparticles. *Adv. Mater.* **2018**, *30*, No. 1704290.

(3) Kwon, S. G.; Piao, Y.; Park, J.; Angappane, S.; Jo, Y.; Hwang, N. M.; Park, J. G.; Hyeon, T. Kinetics of monodisperse iron oxide nanocrystal formation by "heating-up" process. *J. Am. Chem. Soc.* **2007**, *129*, 12571−12584.

(4) Kwon, S. G.; Hyeon, T. Formation mechanisms of uniform nanocrystals via hot-injection and heat-up methods. *Small* **2011**, *7*, 2685−2702.

(5) Boyle, T. J.; Bunge, S. D.; Andrews, N. L.; Matzen, L. E.; Sieg, K.; Rodriguez, M. A.; Headley, T. J. Precursor Structural Influences on the Final ZnO Nanoparticle Morphology from a Novel Family of Structurally Characterized Zinc Alkoxy Alkyl Precursors. *Chem. Mater.* **2004**, *16*, 3279−3288.

(6) Puzder, A.; Williamson, A. J.; Zaitseva, N.; Galli, G.; Manna, L.; Alivisatos, A. P. The effect of organic ligand binding on the growth of CdSe nanoparticles probed by ab initio calculations. *Nano Lett.* **2004**, *4*, 2361−2365.

(7) Manna, L.; Wang, L. W.; Cingolani, R.; Alivisatos, A. P. First-principles modeling of unpassivated and surfactant-passivated bulk facets of wurtzite CdSe: a model system for studying the anisotropic growth of CdSe nanocrystals. *J. Phys. Chem. B* **2005**, *109*, 6183−6192.

(8) van Embden, J.; Mulvaney, P. Nucleation and growth of CdSe nanocrystals in a binary ligand system. *Langmuir* **2005**, *21*, 10226−10233.

(9) Owen, J. S.; Chan, E. M.; Liu, H.; Alivisatos, A. P. Precursor conversion kinetics and the nucleation of cadmium selenide nanocrystals. *J. Am. Chem. Soc.* **2010**, *132*, 18206−18213.

(10) Sayed, F. N.; Polshettiwar, V. Facile and sustainable synthesis of shaped iron oxide nanoparticles: effect of iron precursor salts on the shapes of iron oxides. *Sci. Rep.* **2015**, *5*, 9733.

(11) Hendricks, M. P.; Campos, M. P.; Cleveland, G. T.; Jen-La Plante, I.; Owen, J. S. A tunable library of substituted thiourea precursors to metal sulfide nanocrystals. *Science* **2015**, *348*, 1226−1230.

(12) LaGrow, A. P.; Knudsen, K. R.; AlYami, N. M.; Anjum, D. H.; Bakr, O. M. Effect of Precursor Ligands and Oxidation State in the Synthesis of Bimetallic Nano-Alloys. *Chem. Mater.* **2015**, *27*, 4134−4141.

(13) Frenette, L. C.; Krauss, T. D. Uncovering active precursors in colloidal quantum dot synthesis. *Nat. Commun.* **2017**, *8*, 2082.

(14) Evans, C. M.; Evans, M. E.; Krauss, T. D. Mysteries of TOPSe revealed: insights into quantum dot nucleation. *J. Am. Chem. Soc.* **2010**, *132*, 10973−10975.

(15) Della Gaspera, E.; Chesman, A. S.; van Embden, J.; Jasieniak, J. J. Non-injection synthesis of doped zinc oxide plasmonic nanocrystals. *ACS Nano* **2014**, *8*, 9154−9163.

(16) Kasuya, A.; Sivamohan, R.; Barnakov, Y. A.; Dmitruk, I. M.; Nirasawa, T.; Romanyuk, V. R.; Kumar, V.; Mamykin, S. V.; Tohji, K.; Jeyadevan, B.; Shinoda, K.; Kudo, T.; Terasaki, O.; Liu, Z.; Belosludov, R. V.; Sundararajan, V.; Kawazoe, Y. Ultra-stable nanoparticles of CdSe revealed from mass spectrometry. *Nat. Mater.* **2004**, *3*, 99−102.

(17) Dass, A.; Stevenson, A.; Dubay, G. R.; Tracy, J. B.; Murray, R. W. Nanoparticle MALDI-TOF mass spectrometry without fragmentation: $Au_{25}(SCH_2CH_2Ph)_{18}$ and mixed monolayer $Au_{25}(SCH_2CH_2Ph)_{18-x}L_x$. *J. Am. Chem. Soc.* **2008**, *130*, 5940−5946.

(18) Bakr, O. M.; Amendola, V.; Aikens, C. M.; Wenseleers, W.; Li, R.; Dal Negro, L.; Schatz, G. C.; Stellacci, F. Silver nanoparticles with broad multiband linear optical absorption. *Angew. Chem., Int. Ed.* **2009**, *48*, 5921−5926.

(19) Kim, B. H.; Shin, K.; Kwon, S. G.; Jang, Y.; Lee, H. S.; Lee, H.; Jun, S. W.; Lee, J.; Han, S. Y.; Yim, Y. H.; Kim, D. H.; Hyeon, T. Sizing by weighing: characterizing sizes of ultrasmall-sized iron oxide nanocrystals using MALDI-TOF mass spectrometry. *J. Am. Chem. Soc.* **2013**, *135*, 2407−2410.

https://dx.doi.org/10.1021/acs.inorgchem.0c03567
Inorg. Chem. XXXX, XXX, XXX−XXX

(20) Xie, L.; Shen, Y.; Franke, D.; Sebastian, V.; Bawendi, M. G.; Jensen, K. F. Characterization of Indium Phosphide Quantum Dot Growth Intermediates Using MALDI-TOF Mass Spectrometry. *J. Am. Chem. Soc.* **2016**, *138*, 13469−13472.
(21) Chen, D.; Wang, Q.; Wang, R.; Shen, G. Ternary oxide nanostructured materials for supercapacitors: a review. *J. Mater. Chem. A* **2015**, *3*, 10158−10173.
(22) He, H.; Liao, A.; Guo, W.; Luo, W.; Zhou, Y.; Zou, Z. State-of-the-art progress in the use of ternary metal oxides as photoelectrode materials for water splitting and organic synthesis. *Nano Today* **2019**, *28*, 100763.
(23) Kim, B. H.; Staller, C. M.; Cho, S. H.; Heo, S.; Garrison, C. E.; Kim, J.; Milliron, D. J. High Mobility in Nanocrystal-Based Transparent Conducting Oxide Thin Films. *ACS Nano* **2018**, *12*, 3200−3208.
(24) Kanehara, M.; Koike, H.; Yoshinaga, T.; Teranishi, T. Indium tin oxide nanoparticles with compositionally tunable surface plasmon resonance frequencies in the near-IR region. *J. Am. Chem. Soc.* **2009**, *131*, 17736−17737.
(25) Lounis, S. D.; Runnerstrom, E. L.; Bergerud, A.; Nordlund, D.; Milliron, D. J. Influence of dopant distribution on the plasmonic properties of indium tin oxide nanocrystals. *J. Am. Chem. Soc.* **2014**, *136*, 7110−7116.
(26) Lee, J. H.; Huh, Y. M.; Jun, Y. W.; Seo, J. W.; Jang, J. T.; Song, H. T.; Kim, S.; Cho, E. J.; Yoon, H. G.; Suh, J. S.; Cheon, J. Artificially engineered magnetic nanoparticles for ultra-sensitive molecular imaging. *Nat. Med.* **2007**, *13*, 95−99.
(27) Jang, J. T.; Nah, H.; Lee, J. H.; Moon, S. H.; Kim, M. G.; Cheon, J. Critical enhancements of MRI contrast and hyperthermic effects by dopant-controlled magnetic nanoparticles. *Angew. Chem., Int. Ed.* **2009**, *48*, 1234−1238.
(28) Lee, J. H.; Jang, J. T.; Choi, J. S.; Moon, S. H.; Noh, S. H.; Kim, J. W.; Kim, J. G.; Kim, I. S.; Park, K. I.; Cheon, J. Exchange-coupled magnetic nanoparticles for efficient heat induction. *Nat. Nanotechnol.* **2011**, *6*, 418−422.
(29) Moon, S. H.; Noh, S. H.; Lee, J. H.; Shin, T. H.; Lim, Y.; Cheon, J. Ultrathin Interface Regime of Core-Shell Magnetic Nanoparticles for Effective Magnetism Tailoring. *Nano Lett.* **2017**, *17*, 800−804.
(30) O'Brien, S.; Brus, L.; Murray, C. B. Synthesis of monodisperse nanoparticles of barium titanate: toward a generalized strategy of oxide nanoparticle synthesis. *J. Am. Chem. Soc.* **2001**, *123*, 12085−12086.
(31) Hyeon, T.; Chung, Y.; Park, J.; Lee, S. S.; Kim, Y.-W.; Park, B. H. Synthesis of Highly Crystalline and Monodisperse Cobalt Ferrite Nanocrystals. *J. Phys. Chem. B* **2002**, *106*, 6831−6833.
(32) Bao, N.; Shen, L.; Wang, Y.; Padhan, P.; Gupta, A. A facile thermolysis route to monodisperse ferrite nanocrystals. *J. Am. Chem. Soc.* **2007**, *129*, 12374−12375.
(33) Bao, N.; Shen, L.; An, W.; Padhan, P.; Heath Turner, C.; Gupta, A. Formation Mechanism and Shape Control of Monodisperse Magnetic $CoFe_2O_4$ Nanocrystals. *Chem. Mater.* **2009**, *21*, 3458−3468.
(34) van Embden, J.; Chesman, A. S. R.; Jasieniak, J. J. The Heat-Up Synthesis of Colloidal Nanocrystals. *Chem. Mater.* **2015**, *27*, 2246−2285.
(35) Choi, S. H.; Kim, E. G.; Hyeon, T. One-pot synthesis of copper-indium sulfide nanocrystal heterostructures with acorn, bottle, and larva shapes. *J. Am. Chem. Soc.* **2006**, *128*, 2520−2521.
(36) Choi, S. H.; Kang, Y. C. One-pot facile synthesis of Janus-structured SnO_2-CuO composite nanorods and their application as anode materials in Li-ion batteries. *Nanoscale* **2013**, *5*, 4662−4668.
(37) Liang, W.-I.; Zhang, X.; Bustillo, K.; Chiu, C.-H.; Wu, W.-W.; Xu, J.; Chu, Y.-H.; Zheng, H. In Situ Study of Spinel Ferrite Nanocrystal Growth Using Liquid Cell Transmission Electron Microscopy. *Chem. Mater.* **2015**, *27*, 8146−8152.
(38) Chang, H.; Kim, B. H.; Jeong, H. Y.; Moon, J. H.; Park, M.; Shin, K.; Chae, S. I.; Lee, J.; Kang, T.; Choi, B. K.; Yang, J.; Bootharaju, M. S.; Song, H.; An, S. H.; Park, K. M.; Oh, J. Y.; Lee, H.; Kim, M. S.; Park, J.; Hyeon, T. Molecular-Level Understanding of Continuous Growth from Iron-Oxo Clusters to Iron Oxide Nanoparticles. *J. Am. Chem. Soc.* **2019**, *141*, 7037−7045.
(39) Park, J.; An, K.; Hwang, Y.; Park, J. G.; Noh, H. J.; Kim, J. Y.; Park, J. H.; Hwang, N. M.; Hyeon, T. Ultra-large-scale syntheses of monodisperse nanocrystals. *Nat. Mater.* **2004**, *3*, 891−895.
(40) An, K.; Lee, N.; Park, J.; Kim, S. C.; Hwang, Y.; Park, J. G.; Kim, J. Y.; Park, J. H.; Han, M. J.; Yu, J.; Hyeon, T. Synthesis, characterization, and self-assembly of pencil-shaped CoO nanorods. *J. Am. Chem. Soc.* **2006**, *128*, 9753−9760.
(41) Long, G. J.; Robinson, W. T.; Tappmeyer, W. P.; Bridges, D. L. The magnetic, electronic, and Mössbauer spectral properties of several trinuclear iron(III) carboxylate complexes. *J. Chem. Soc., Dalton Trans.* **1973**, 573−579.
(42) Thich, J. A.; Toby, B. H.; Powers, D. A.; Potenza, J. A.; Schugar, H. J. Magnetic properties of $K_5[(H_2O)_3(SO_4)_6Fe_3O].6H_2O$, a sulfate analog of the trimeric basic iron(III) carboxylates. *Inorg. Chem.* **1981**, *20*, 3314−3317.
(43) Johnson, M. K.; Powell, D. B.; Cannon, R. D. Vibrational spectra of carboxylato complexes—III. Trinuclear 'basic' acetates and formates of chromium(III), iron(III) and other transition metals. *Spectrochim. Acta, Part A* **1981**, *37*, 995−1006.
(44) Oh, S. M.; Hendrickson, D. N.; Hassett, K. L.; Davis, R. E. Electron transfer in mixed-valence, oxo-centered, trinuclear iron acetate complexes: effect of statically disordered to dynamically disordered transformation in the solid state. *J. Am. Chem. Soc.* **1984**, *106*, 7984−7985.
(45) Oh, S. M.; Henderickson, D. N.; Hassett, K. L.; Davis, R. E. Valence-detrapping modes for electron transfer in the solid state of mixed-valence, oxo-centered, trinuclear iron acetate complexes: x-ray structure and physical data for $[Fe_3O(O_2CCH_3)_6(4\text{-Et-py})_3](4\text{-Et-py})$. *J. Am. Chem. Soc.* **1985**, *107*, 8009−8018.
(46) Blake, A. B.; Yavari, A.; Hatfield, W. E.; Sethulekshmi, C. N. Magnetic and spectroscopic properties of some heterotrinuclear basic acetates of chromium(III), iron(III), and divalent metal ions. *J. Chem. Soc., Dalton Trans.* **1985**, 2509−2520.
(47) Nakamoto, T.; Hanaya, M.; Katada, M.; Endo, K.; Kitagawa, S.; Sano, H. The Valence-Detrapping Phase Transition in a Crystal of the Mixed-Valence Trinuclear Iron Cyanoacetate Complex $[Fe_3O(O_2CCH_2CN)_6(H_2O)_3]$. *Inorg. Chem.* **1997**, *36*, 4347−4359.
(48) Sanchez-Lievanos, K. R.; Tariq, M.; Brennessel, W. W.; Knowles, K. E. Heterometallic trinuclear oxo-centered clusters as single-source precursors for synthesis of stoichiometric monodisperse transition metal ferrite nanocrystals. *Dalton Trans.* **2020**, *49*, 16348−16358.
(49) Montri, L.; Cannon, R. D. Vibrational spectra of carboxylato complexes—V. Vibrations of the bridging oxide ion in the trinuclear complex $[Fe_3O(OOCCH_3)_6(C_5H_5N)_3]^+$. *Spectrochim. Acta, Part A* **1985**, *41*, 643−646.
(50) Meesuk, L.; Jayasooriya, U. A.; Cannon, R. D. Vibrational spectra of carboxylate complexes. VII. Partial valence trapping in a trinuclear mixed-valence iron(III,III,II) cluster: vibrational spectra of $[Fe_3O(OOCCH_3)_6L_3]$ and related mixed-metal complexes. *J. Am. Chem. Soc.* **1987**, *109*, 2009−2016.
(51) Kim, Y. H.; Kang, Y. S.; Lee, W. J.; Jo, B. G.; Jeong, J. H. Synthesis of Cu Nanoparticles Prepared by Using Thermal Decomposition of Cu-oleate Complex. *Mol. Cryst. Liq. Cryst.* **2006**, *445*, 231−238.
(52) Morrow, L.; Barron, A. R. Issues Affecting the Synthetic Scalability of Ternary Metal Ferrite Nanoparticles. *J. Nanopart.* **2015**, *2015*, 1−8.
(53) Atkins, P. W.; Paula, J. D. *Atkins' Physical Chemistry*, 9th ed.; Oxford University Press, 2010.

https://dx.doi.org/10.1021/acs.inorgchem.0c03567
Inorg. Chem. XXXX, XXX, XXX−XXX